Solar Energy Materials and Solar Cells 195 (2019) 55–62

Contents lists available at ScienceDirect

Solar Energy Materials and Solar Cells

journal homepage: www.elsevier.com/locate/solmat

Influencing mechanism of cationic ratios on efficiency of $Cu_2ZnSn(S,Se)_4$ solar cells fabricated with DMF-based solution approach

Hongmei Luan[a,b], Bin Yao[a,b,*], Yongfeng Li[a,b,*], Ruijian Liu[b], Zhanhui Ding[a,b], Yingrui Sui[c], Zhenzhong Zhang[d], Haifeng Zhao[d], Ligong Zhang[d]

[a] State Key Lab of Superhard Material, and College of Physics, Jilin University, Changchun 130012, China
[b] Key Laboratory of Physics and Technology for Advanced Batteries (Ministry of Education), College of Physics, Jilin University, Changchun 130012, China
[c] Key Laboratory of Functional Materials Physics and Chemistry of the Ministry of Education, Jilin Normal University, Changchun130103, China
[d] State Key Laboratory of Luminescence and Applications, Changchun Institute of Optics, Fine Mechanics and Physics, Chinese Academy of Sciences, No.3888 Dongnanhu Road, Changchun 130033, China

ARTICLE INFO

Keywords:
Solar cell
CZTSSe
DMF
Interfacial recombination
Interfacial structure
Cationic ratios

ABSTRACT

In the present work, kesterite $Cu_2ZnSn(S,Se)_4$ (CZTSSe) films were successfully prepared by tuning the cationic ratios (Zn/Sn and Cu/(Zn + Sn)) with DMF-based solution approach and the effect of cationic ratios on the performance of solar cells with the CZTSSe as absorbers was studied. Our results revealed that the interfacial secondary phases and interfacial structure of CZTSSe/Mo can be optimized by changing the cationic ratios so as to decrease the reverse saturation current (J_0) and increase the shunt resistance (R_{sh}). And the photocurrent (J_L) can be improved by broadened depletion region layer (W_d) of the solar cell due to decreased net hole concentration (N_B) induced by decreased Cu/(Zn + Sn). By optimizing the cationic ratios, the CZTSSe solar cell with the highest power conversion efficiency (PCE) of 8.01% was obtained at Cu/(Zn + Sn) = 0.75 ± 0.05 and Zn/Sn = 1.18 ± 0.02. The increase of PCE is mainly attributed to the decrease of interfacial secondary phases and the improvement of interfacial structure.

1. Introduction

$Cu(In,Ga)Se_2$ and CdTe are both attractive materials as the stable absorber of thin film solar cell. However, concern over the use of expensive or toxic elements such as indium (In)/gallium (Ga) and cadmium (Cd) prompts researchers to seek for an alternative material. Among the various candidates, $Cu_2ZnSn(S,Se)_4$ (CZTSSe) is composed of earth-abundant elements and of low toxicity, which is therefore more appropriate for mass production. So far, CZTSSe thin film solar cell with world-record power conversion efficiency (PCE) of 12.6% has been reported by the David B. Mitzi group [1], which was fabricated based on hydrazine solution. Nowadays, a variety of solvent have been proposed, such as dimethyl sulfoxide (DMSO) [2–4], ethylene glycol monoethylether (EGME) [5–8], water-ethanol [9,10], 1,3-dimethyl-2-imadazolidinone(DMI) [11], N, N-dimethyl formamide (DMF) [12], and so on [13]. Among of them, the DMF is very stable and can be used without any thickeners. These are helpful to precisely tune the composition of CZTSSe and reduce the effect of residual carbon on the interface of back electrode, and thus improve the quality and performance of solar cells. However, only a few literatures reported adopted DMF-based solution approach to prepare CZTSSe solar cells. Up to now, Liu et al.[12] have reported the Cu_2ZnSnS_4 (CZTS) solar cell prepared by DMF-based solution approach and the reliable record of PCE is merely 4.77%. Schnabel et al. [14] fabricated 5.1% PCE solar cells using Ge-doped CZTSSe as the absorber, and the highest PCE can reach 11% by Collord et al. [15]. These results demonstrate that the DMF is a hopeful process of preparation of CZTSSe solar cell with high PCE, and further research is needed.

It is well known that a single-phase CZTSSe is necessary to obtain CZTSSe solar cells with high performance, but it is fairly hard due to the tiny region that allows the chemical composition of pure CZTSSe to change. Therefore, Hironori Katagiri group first proposed to optimize the cationic ratio of Cu/(Zn + Sn) or Zn/Sn in CZTS absorber using sputtering approach aiming to improve the PCE of solar cell [16]. Subsequently, Shiyou Chen group have deduced from first-principles approach that the Cu poor and Zn rich conditions (that is, cationic ratios are Cu/(Zn + Sn) ≈ 0.8 and Zn/Sn ≈ 1.2) is necessary to obtain higher solar cell performance [17]. However, we noted that the cationic composition of CZTSSe in their best solar cells varies a lot with different approaches, which indicates that the optimal cationic composition of

* Corresponding authors at: State Key Lab of Superhard Material, and College of Physics, Jilin University, Changchun 130012, China.
E-mail addresses: binyao@jlu.edu.cn (B. Yao), liyongfeng@jlu.edu.cn (Y. Li).

https://doi.org/10.1016/j.solmat.2019.02.029
Received 25 November 2018; Received in revised form 23 February 2019; Accepted 24 February 2019

CZTSSe may be not same for different methods due to some inevitable imperfections within them. For example, Yi Zhang group have reported that the cationic ratio of Zn/Sn is 1.02 for CZTSe solar cells prepared by DC-magnetron sputtering [18] while Stefan G. Haass group disclosed the optimal cationic ratios of Cu/(Zn + Sn) and Zn/Sn are respectively 0.90 ± 0.03 and 1.27 ± 0.04 for DMSO solution process [2]. In addition, some reports indicated that the optimal ratios of Cu/(Zn + Sn) and Zn/Sn are respectively 0.85 and 1.25 for EGME [6] while 0.81 and 1.28 for water-based solution process [10]. In fact, it can be expected that the rate for same chemical reaction in different solvents should be different owing to their different reaction environments. Up to now, the cationic ratios of CZTSSe prepared by solution approach has not been systematically investigated and the optimal cationic composition remains unclear, which has important influence on the optical and electrical properties of CZTSSe solar cells. The cationic ratios also have a significant influence on interfacial recombination, built-in field and formation of a single-phase kesterite CZTSSe. These effects have been demonstrated to be important for preparation of high PCE CZTSSe solar cell [18–21]. However, the research work about the effect of cationic ratios on interfacial recombination and built-in field is scarcely reported.

In the present work, single-phase kesterite CZTSSe films were prepared with different nominal cationic ratios of Zn/Sn using DMF-based solution approach, and the corresponding CZTSSe solar cells were also fabricated. The superiority of DMF as a solvent was discussed and the effect of cationic ratios on the performance of solar cell was studied. Meanwhile, we made an explicit depiction about how the cationic ratios affect the depletion region width (W_d) and back electrode interface based on our experimental results. By optimizing the atomic ratios, the PCE of CZTSSe solar cell reaches 8.01%, to our knowledge, which is the highest value for CZTSSe solar cell prepared with the DMF-based solution approach.

2. Experimental

Cu-Zn-Sn-S precursor solutions with nominal cationic ratios of Cu/(Zn + Sn) = 0.7 and Zn/Sn = 1.05–1.30 were prepared by dissolving Cu $(CH_3COO)_2 \cdot H_2O$, $SnCl_2 \cdot 2H_2O$, $ZnCl_2$, and thiourea into DMF (1.22 M) solvent and then magnetically stirring for 3 h at room temperature. In order to get CZTSSe films with different chemical composition, the cationic ratios were adjusted by increasing the amount of the Cu(II) and Zn(II) salts while keeping the amount of Sn(II) salt as a constant (3.3 mmol). These precursor solutions were denoted as S-x (x = I, II, III, IV, V and VI), as listed in Table 1. Obviously, the concentration of Sn ion decreases with increasing Zn/Sn ratio in the precursor solutions. Subsequently, the CZTS precursor films were prepared by spin-coating the precursor solutions onto the Molybdenum-coated soda-lime glass substrate at a rotating rate of 3000 rpm followed by drying at 300 °C for 3 min in a N_2-filled glovebox (Mikrouna universal style glovebox). The coating and drying processes were repeated 10 times to obtain 1.4 µm-thick CZTS precursor films [12,22]. To get the suitable CZTSSe thin films, the CZTS precursor films and some selenium granules were sealed in a graphite box, followed by annealing for 15 min at 550 °C and 1 bar in a rapid thermal processing (RTP) furnace under N_2 flow of 50 ml/min with a heating rate of 4 °C/s, and finally cooled down to room temperature naturally. All of the CZTSSe films were etched by $KMnO_4$/H_2SO_4 + Na_2S to remove their possible ZnSe surface secondary phase [23]. The CZTSSe films corresponding to the S-x (x = I-VI) are denoted as CZTSSe-x (x = I-VI), respectively. The cationic ratios of CZTSSe films were measured by EDS and are listed in Table 1. It is noted that the Cu/(Zn + Sn) ratios are larger in the CZTSSe films than in precursor solution while Zn/Sn ratios of the CZTSSe films are larger than or equal to that of the precursor solutions, which imply that some Sn and Zn lose during selenization process.

Using the CZTSSe-x (x = I-VI) as absorbers, solar cells were fabricated with a conventional structure of glass/Mo/CZTSSe/CdS/i-ZnO/ITO/Al. The CdS buffer layer was prepared by chemical bath deposition, using $CdSO_4 \cdot 8/3H_2O$ as cadmium precursor sources [24,25], followed by the radio frequency magnetron sputtering deposition of i-ZnO (~50 nm) and ITO (~260 nm) on the top of CdS. An Aluminum top contact was then deposited through a metal mask using thermal evaporation method. Finally, the devices were mechanically isolated with an active area of 0.19 cm^2. The solar cells with CZTSSe-x(x = I-VI) as absorbers hereafter are referred to as Cell-x (x = I-VI), respectively.

The crystal structures of CZTSSe films were characterized by an X-ray diffractometer (XRD) with Cu K_α radiation (λ = 1.5406 Å). The composition of CZTSSe films and the cross-sectional morphologies of CZTSSe-based solar cells were measured by scanning electron microscope (SEM) (Hitachi S-4800) equipped with an energy-dispersive X-ray spectroscopy (EDS) system (EDAX Genesis 2000). The current density-voltage (J-V) curves were collected via a solar simulator (SAN-EI, XES-40S2-CE; AM 1.5) and a Keithley 2400 SourceMeter. The light intensity of the solar simulator illuminated was calibrated to 100 mW/cm^2 on devices. C-V curves were measured with a Keithley 4200-SCS instrument under dark condition. Note that the frequency of 100 Hz and ac amplitude of 30 mV were applied for C-V measurement. C-V measurement was taken under 1 to −1 V reverse bias at 300 K. The external quantum efficiency (EQE) spectra were measured by a Zolix SCS100 QE system. The EQE was measured wavelength from 300 to 1400 nm with an in-house setup using chopped monochromatic light, lock-in detection, and no white light bias. The temperature-dependent current density-voltage measurements were performed in a temperature ranging from 10 K to 300 K by using an 8200 compressor and a CTI-CRYOGENICS cryostat.

3. Results and discussion

Fig. 1 shows the technological process for the preparation of CZTS precursor solution. It has been reported that CZTS precursor solution usually shows yellow color due to existence of unreacted Cu^{2+} which can form $CuCl_4^{2-}$ (a yellow species) if the concentration of Cl^- within solution is very high [4,12,14,26]. However, the precursor solutions we prepared show light primrose yellow and even colorless, and moreover have not any change as they were sealed in vials and placed for one month, as shown in Fig. 1. These results indicate that our precursor solutions are stable and have lower concentration of Cu^{2+} than those

Table 1
The ratios of Cu/(Zn + Sn) and Zn/Sn of the precursor solutions and corresponding CZTSSe films.

Number of samples	Precursor solution (mol/L)						CZTSSe films (at%)		
	Solutions	Cu (M)	Zn (M)	Sn (M)	Cu/ (Zn + Sn)	Zn/Sn	Films	Cu/ (Zn + Sn)	Zn/Sn
3	S-I	0.50	0.36	0.36	0.70	1.05	CZTSSe-I	0.84 ± 0.03	1.16 ± 0.03
3	S-II	0.50	0.37	0.35	0.70	1.10	CZTSSe-II	0.82 ± 0.02	1.14 ± 0.04
3	S-III	0.50	0.38	0.34	0.70	1.15	CZTSSe-III	0.81 ± 0.04	1.28 ± 0.03
4	S-IV	0.50	0.38	0.33	0.70	1.20	CZTSSe-IV	0.75 ± 0.05	1.18 ± 0.02
3	S-V	0.50	0.39	0.32	0.70	1.25	CZTSSe-V	0.78 ± 0.02	1.19 ± 0.05
3	S-VI	0.50	0.40	0.31	0.70	1.30	CZTSSe-VI	0.76 ± 0.03	1.30 ± 0.05

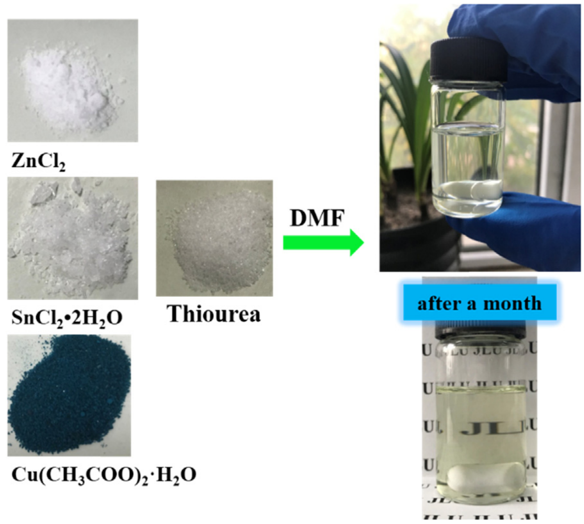

Fig. 1. The technological process for the preparation of CZTS precursor solution with DMF as the solvent.

yellow solutions reported previously [4,12,14,26], which is favorable to composition control and crystal quality improvement of CZTSSe film.

Fig. 2 shows the XRD patterns of CZTSSe-x (x = I-VI). The diffraction peaks from Mo are around 40.53° and 73.50°. The hump around 11.88° is ascribed to the organic glass holder. The peaks labeled ♥ are in agreement with (101) and (110) peaks of Mo(S,Se)$_2$, respectively, indicating the formation of Mo(S,Se)$_2$ at CZTSSe/Mo interface. The diffraction peaks marked by ◆ are attributed to kesterite CZTSSe (PDF #97-009-5117). The XRD peaks marked by • are due to Sn(S,Se)$_2$ secondary phase (PDF#23–0602). It is found from Fig. 2 that the CZTSSe-I and CZTSSe-II are dual phase polycrystals composed of CZTSSe and Sn(S,Se)$_2$ while the CZTSSe-III~CZTSSe-VI only contain the phase CZTSSe. These mean that a single-phase CZTSSe can be formed at the ratio of Cu/(Zn + Sn) = 0.76–0.81 and Zn/Sn = 1.18–1.30, as shown in Table 1 and Fig. 2c–f. The formation of Sn(S,Se)$_2$ is due to that the contents of Sn^{4+} in S-I and -II precursor solutions deviate from its stoichiometry in Kesterite CZTSSe phase. The sharp diffraction peaks imply the good crystalline quality of CZTSSe films.

The J-V curves of Cell-x (x = I-VI) are shown in Fig. 3a and corresponding performance parameters are listed in Table 2. It can be obviously seen that the PCE, open-circuit voltage (V_{oc}), short-circuit current density (J_{sc}) and fill factor (FF) change with the cationic ratios of CZTSSe absorbers. The highest PCE of 8.01% with V_{oc} of 417 mV, J_{sc} of 36.78 mA/cm^2 and FF of 52.27% is obtained for Cell-IV with the ratios of Cu/(Zn + Sn) = 0.75 ± 0.05 and Zn/Sn = 1.18 ± 0.02, which are slightly different from the optimal ratios of Cu/(Zn + Sn) = 0.90 ± 0.03 and Zn/Sn = 1.27 ± 0.04 in DMSO-based solution approach reported previously in literatures [27–30] and closed to the reported result of Chen et al. [17]. For the credibility of the data, the statistics data of performance parameters of the Cell-x (x = I-VI) are depicted in Fig. S1 of supporting information, which show the same change tendency as Table 2. Fig. 3b shows the external quantum efficiency (EQE) spectra of the Cell-x (x = I-VI). The plots of $[h\nu \times \ln(1-EQE)]^2$ as a function of hν are shown in the inset of Fig. 3b, from which the band gaps (E_g) of Cell-I, Cell-II, Cell-II, Cell-IV, Cell-V and Cell-VI were estimated to be 1.100, 1.081, 1.096, 1.065, 1.081 and 1.059 eV, respectively. As we know, V_{oc} increases with increasing E_g. However, it can be found from Table 2 that the V_{oc} does not increase with increasing E_g but even decrease. This indicates the change of the V_{oc} is not mainly from E_g but electrical parameters of the solar cells [37]. In addition, EQE of the solar cells are same in the short wavelength range (< 600 nm) but very different in the long wavelength range (> 600 nm), which also comes from electrical parameters [31].

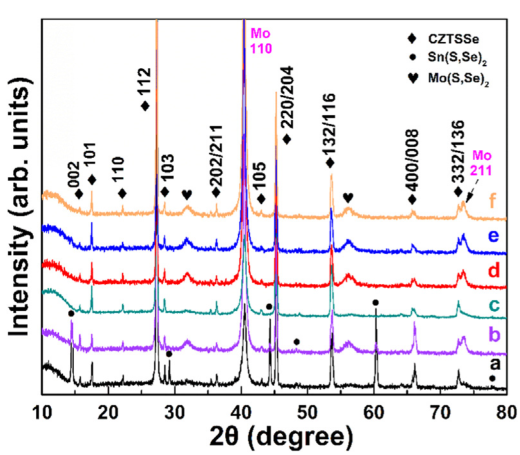

Fig. 2. XRD patterns of the CZTSSe-I (a), -II (b), -III (c), IV (d), -V (e), and -VI (f).

The electrical parameters of Cell-x (x = I-VI), including shunt resistance (R_{sh}), series resistance (R_s), diode ideality factor (A) and reverse saturation current (J_0) are derived from the J-V curves by site's method [32,33], as listed in Table 2. It is well known that the decrease in R_s and J_0 as well as the increase in R_{sh} are beneficial to increase in the performance parameters. It can be seen that the variation of J_0 keeps the exactly same pace with V_{oc} and J_{sc} while variation of R_{sh} with FF, which indicates that the V_{oc}, J_{sc} and FF are dominantly related to the recombination and R_{sh} of Cell-x. The recombination dominantly occurs at the interface because the value of A is larger than 2 [32,34–36].

In order to figure out the recombination mechanism, temperature-dependent J-V measurement was carried out from 10 to 300 K for the Cell-x (x = I-VI) and the derived V_{oc} is plotted as a function of temperature in Fig. 4. It can be found that the V_{oc} is linearly dependent on the temperature in the range of 125–300 K. It is known that the temperature dependence of V_{oc} can be presented as [37,38],

$$V_{oc} = \frac{E_a}{q} - \frac{AkT}{q}\ln\left(\frac{J_{00}}{J_L}\right) \tag{1}$$

where J_L, E_a, A, k are the photocurrent, activation energy, diode ideality factor and Boltzmann constant, respectively. The constant q is the electrical charge of an electron and J_{00} is prefactor of reverse saturation current. In general, E_a heavily depends on the recombination type in the solar cell and can be derived by extrapolating the linear part of V_{oc} to 0 K. The E_a would be close to the band gaps of absorber (E_g) in the case of bulk recombination but smaller than E_g in the case of interfacial recombination [33,39]. The larger difference between E_g-E_a(denoted as ΔE_{ga}) implies higher interfacial recombination.

As shown in Fig. 4, by linear fitting the derived values of E_a are 0.659, 0.736, 0.835, 0.922, 0.796 and 0.686 eV for Cell-I~Cell-VI, respectively. E_a of each solar cell is smaller than its E_g, confirming that interfacial recombination is dominant. By using E_g obtained from Fig. 3b, the ΔE_{ga} of each solar cell can be calculated. Combing the J_0 of each solar cell in Table 2, the dependence of the J_0 on the ΔE_{ga} is plotted in Fig. 5a, indicating that the J_0 increases with increasing ΔE_{ga}. This demonstrates that the J_0 mainly comes from contribution of interfacial recombination. It is found from Fig. 5b–d that the PCE, J_{sc} and V_{oc} decreases with the increasing ΔE_{ga}, demonstrating that interfacial recombination have a negative effect on PCE, J_{sc} and V_{oc} of CZTSSe solar cell [40–42].

It is well known that R_{sh} and interfacial recombination are related to defects and secondary phases formed in the p-n junction of CdS/CZTSSe and at CZTSSe/Mo interfaces, such as, Zn(S,Se) and Sn(S,Se)$_2$ etc [43]. In the p-n junction, the formation of defects and secondary phases is due to deviation of Zn/Sn and Cu/(Zn + Sn) ratios from stoichiometric

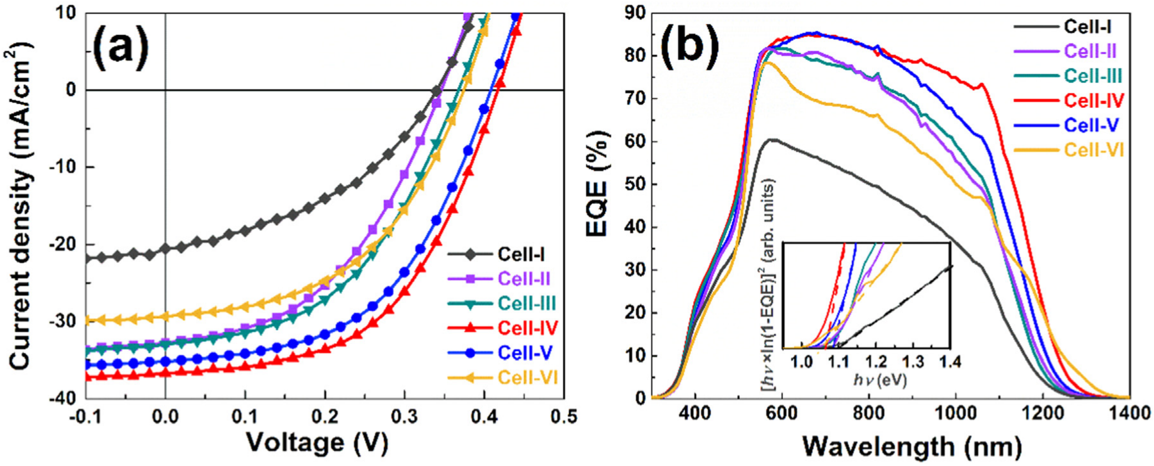

Fig. 3. (a) J-V curves and (b) the EQE of Cell-x (x = I, II, III, IV, V and VI). The inset in (b) is the plot of $[h\nu \times \ln(1\text{-EQE})]^2$ as a function of $h\nu$.

ratio of single-phase CZTSSe. Fig. 6a–c reveals that the ΔE_{ga}, R_{sh} and J_0 increase with increasing Cu/(Zn+Sn) ratio, demonstrating that they are related to Cu/(Zn+Sn) and Zn/Sn ratios. As shown in Table 2 and Fig. 6a–c, R_{sh} is the highest and J_0 is the smallest at Zn/Sn of near 1.18 and Cu/(Zn+Sn) of near 0.75, implying that the amount of defects and secondary phases is the least in Cell-IV. In addition, it is also found that the surface of CZTSSe-IV are more smoothing and without voids than that of CZTSSe with the rest, as shown in Fig. S2 in supporting information, which also has contribution to the increased R_{sh} and decreased J_0.

For the CZTSSe/Mo interface, the formation of secondary phases is mainly related to the reaction between CZTSSe and Mo layers during annealing process which can be described by following equation.

$$2Cu_2ZnSn(S, Se)_4 + Mo \xrightarrow{\text{annealing}} 2Cu_2(S, Se) + 2Zn(S, Se) + Sn(S, Se) + Mo(S, Se)_2 \quad (1')$$

So, CZTSSe/Mo interface may has more secondary phases than CdS/CZTSSe [44,45].

Besides the secondary phases, interfacial structure of CZTSSe/Mo may also have influence on interfacial recombination. Fig. 7 shows the cross-sectional SEM images of Cell-x (x = I-VI). It can be seen that the thicknesses of the CZTSSe in the six solar cells are larger than 1 µm, which means that the decrease of J_{sc} with increasing wavelength in the long wavelength rang comes from electrical loss rather than the deficient light absorption [33,46,47]. Although the absorbers of the six solar cells consist of larger grains, the Cell-x has different absorber/Mo interfacial structures. The Cell-I and Cell-II have many small void (marked by red circles) near the CZTSSe/Mo interface besides a thin-layer $Mo(S,Se)_2$, as shown in Fig. 7a and b, which results in large J_0. Cell-III has a thin-layer $Mo(S,Se)_2$ and a bi-absorber structure as reported previously [22,48–52], as shown in Fig. 7c. This bi-absorber also can improve the value of J_0. It can be seen from Fig. 7d and e that the absorber contacts with Mo closely and is composed of large, densely packed, crack-free and lengthways grains. These make the Cell-IV and -V have smaller J_0 than other solar cells, as listed in Table 2. However, Fig. 7f shows that the Cell-VI has not only thick-layer $Mo(S,Se)_2$ but also a distinct bi-absorber structure with a small-grain bottom layer and some voids at the CZTSSe/Mo interface, which make the J_0 much larger than that of Cell-II~V. This may explain why the J_0 of the Cell-VI is much larger than that of Cell-II~V, as shown in Fig. 6c, although its Cu/(Zn+Sn) ratio is smaller than that of Cell-II, -III, -V and very closed to that of Cell-IV.

Above results indicate that the interfacial recombination is related to the structure of CZTSSe/Mo interface as well as the defects and secondary phases in the p-n junction and at CZTSSe/Mo interface, which can be optimized by tuning the cationic ratios of CZTSSe.

It is known that another important factor affecting V_{oc} and J_{sc} besides electrical parameters is J_L, which is related to the W_d. In order to determine the W_d of the six solar cells, C-V measurement was performed. Fig. 8 shows the corresponding C-V and C^{-2}-V curves. According to the Mott–Schottky equation, the net hole concentration (N_B) can be calculated by: $N_B = 2/(qK_sS^2[d(1/C^2)/dV])$, where q is the electron charge, K_s is the semiconductor dielectric constant (K_s is fixed to be 8 in this work) [53,54], and S is the device area. While the W_d was calculated with formula $W_d = (2K_sV_{bi}/qN_B)^{1/2}$, that V_{bi} is the built-in electric field. The N_B and W_d of CZTSSe solar cells can be derived from the C^{-2}-V relations according to the method reported in previous literature [33], and the V_{bi}, N_B and W_d of the Cell-x (x = I-VI) are listed in Table 3.

Combining Tables 1 and 3, it is concluded that the net hole concentrations (N_B) increases with the increasing Cu/(Zn+Sn), as shown in Fig. 6d, which is in agreement with the theoretical research [17]. This means that the N_B mainly comes from the contribution of Cu_{Zn} antisites in CZTSSe and the density of Cu_{Zn} can be tuned by Cu/(Zn+Sn) ratios.

It is well known that increased W_d can promote separation ability of photogenerated electron-hole pairs, resulting in increment in V_{oc} and J_{sc}. Table 3 shows that the ranking order of W_d in six solar cells is Cell-IV > Cell-V > Cell-VI > Cell-III > Cell-II > Cell-I. Obviously, the W_d of Cell-IV is much larger than that of others. These results indicate that the

Table 2
Performance and electrical parameters of CZTSSe-based solar cells.

Samples	J_{sc} (mA/cm^2)	V_{oc}(V)	PCE %	FF %	R_s (Ω cm^2)	R_{sh} (Ω cm^2)	G (mS/cm^2)	A	J_0 (mA/cm^2)
Cell-I	20.60	0.341	2.87	40.98	0.51	250.00	4.00	3.50	0.60
Cell-II	32.78	0.340	5.12	45.94	1.52	359.70	2.78	2.60	0.22
Cell-III	32.90	0.367	5.69	47.10	1.80	456.60	2.19	2.52	0.13
Cell-IV	36.70	0.417	8.01	52.27	1.49	520.80	1.92	2.34	0.04
Cell-V	35.23	0.400	7.31	51.87	1.63	581.40	1.72	2.44	0.07
Cell-VI	29.39	0.371	5.33	48.88	0.77	465.12	2.15	3.07	0.27

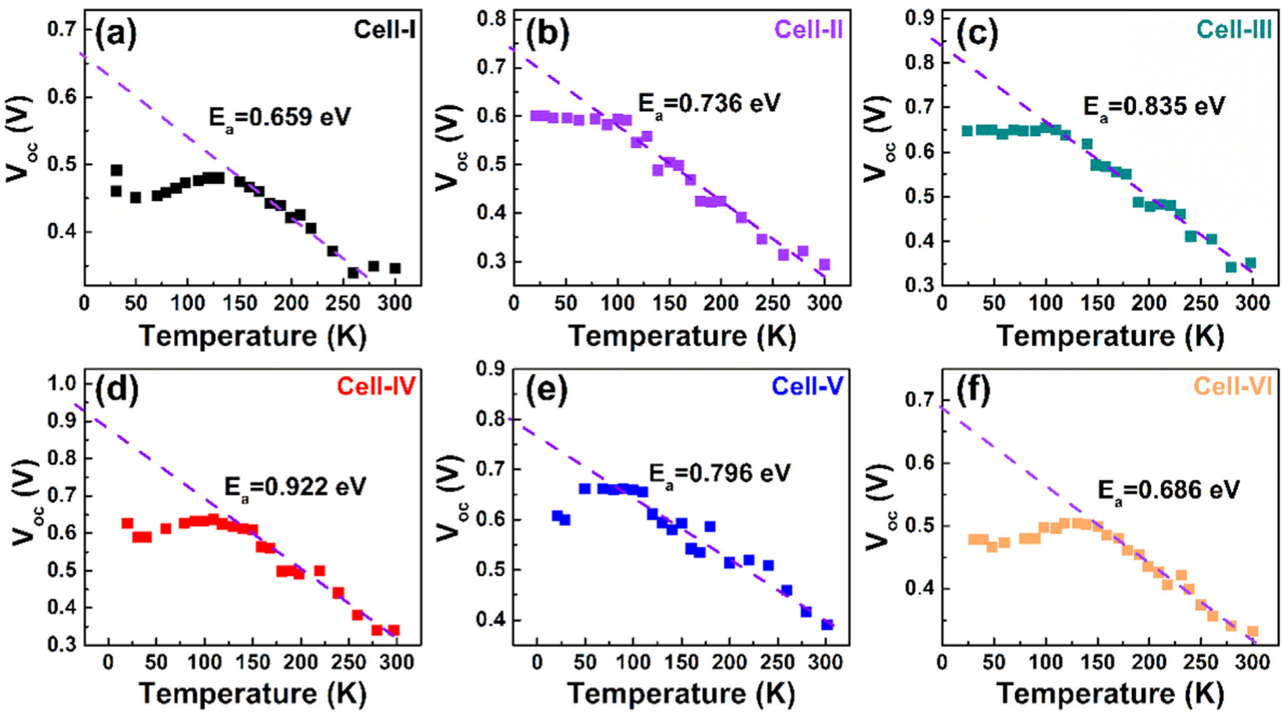

Fig. 4. The temperature-dependent V_{oc} under simulated 1 sun illumination for (a) Cell-I, (b) Cell-II, (c) Cell-III, (d) Cell-IV, (e) Cell-V and (f) Cell-VI.

J_L of six solar cells ranks in the same order as W_d, and J_L of the Cell-IV is the highest, in agreement with the V_{oc} and J_{sc} results. These results reveal that the J_L induced by the change of the cationic composition also contributes a lot to the change of V_{oc} and J_{sc}.

4. Conclusion

A single-phase kesterite CZTSSe was prepared at the cationic ratios of Cu/(Zn + Sn) = 0.75–0.81 and Zn/Sn = 1.18–1.30 by DMF-based solution approach. CZTSSe-based solar cells with conventional structure were fabricated with the CZTSSe as absorbers. The PCE, V_{oc}, J_{sc} and FF can be changed with the cationic ratios and this change has been

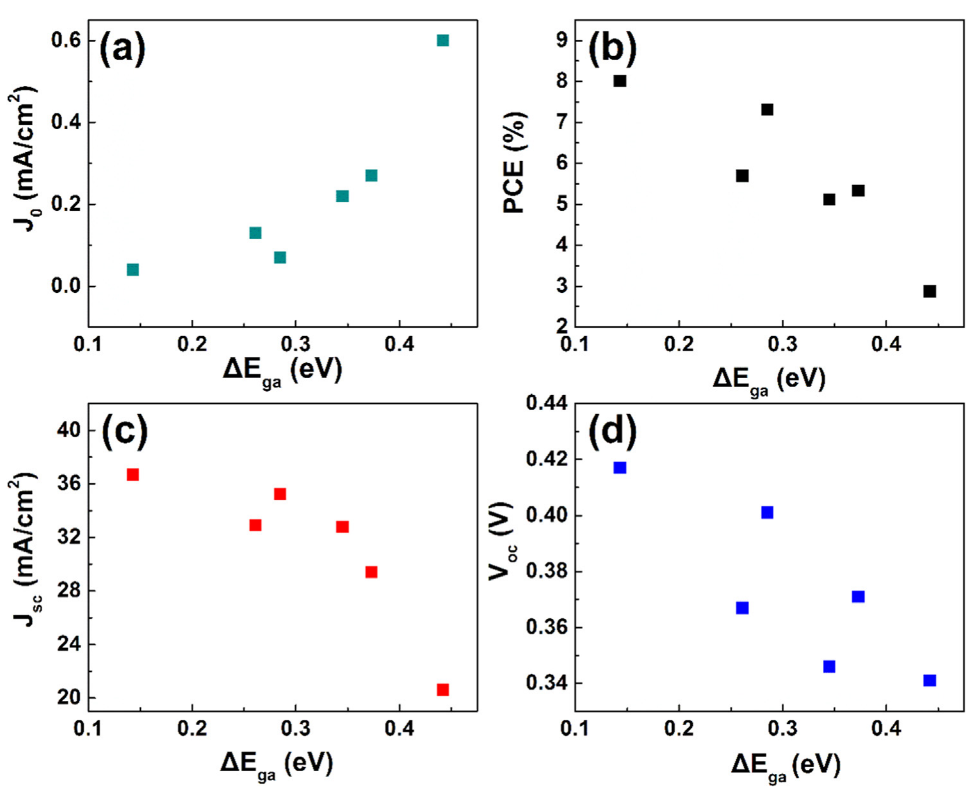

Fig. 5. (a) The plots of J_0 vs the difference between E_g and E_a (ΔE_{ga}), (b) the PCE vs ΔE_{ga}, (c) the J_{sc} vs ΔE_{ga} and (d) the V_{oc} vs ΔE_{ga} of Cell-x solar cells.

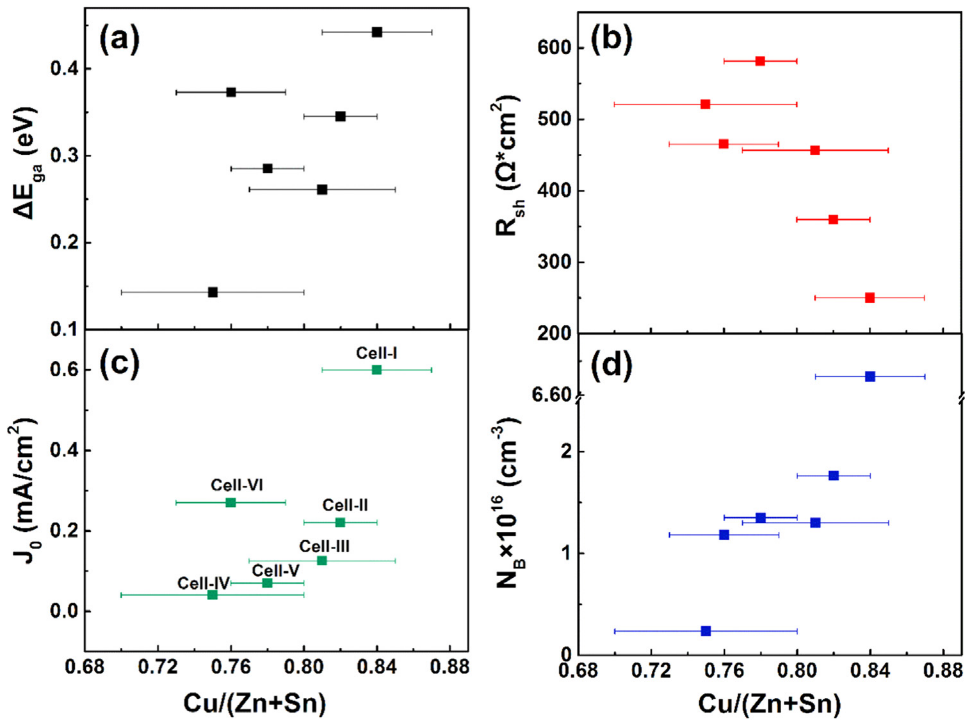

Fig. 6. (a) The plots of the difference between E_g and E_a (ΔE_{ga}) vs Cu/(Zn + Sn) ratios with the error bars. (b) the plots of the R_{sh} vs Cu/(Zn + Sn) ratios, (c) the J_0 vs Cu/(Zn + Sn) ratios and (d) the N_B vs Cu/(Zn + Sn) ratios of Cell-x solar cells.

demonstrated to be mainly caused by J_0, R_{sh} and J_L. The R_{sh} is determined mainly by interfacial secondary phases, the J_0 is dominated by interfacial recombination induced by defects, secondary phases in the p-n junction and at CZTSSe/Mo as well as the structure of CZTSSe/Mo interface, while the J_L is determined by W_d. The defects, secondary phases, interfacial structure and W_d can be adjusted by tuning the cationic composition. By optimizing the cationic ratio, a CZTSSe solar cell with highest PCE of 8.01% is obtained at the ratios of Cu/(Zn + Sn) = 0.75 ± 0.05 and Zn/Sn = 1.18 ± 0.02, due to its largest W_d and the best interfacial structure, where the CZTSSe is a single layer with large grain size, void-free and close contact with Mo electrode.

Acknowledgement

This work is supported by the National Natural Science Foundation of China under Grant Nos. 61774075, 11274135, 61604029 and 61505067, The Science and Technology Development Project of Jilin Province under grant No. 20170101142JC, Specialized Research Fund for the Doctoral Program of Higher Education under Grant no. 20130061130011, and Ph.D. Programs Foundation of Ministry of

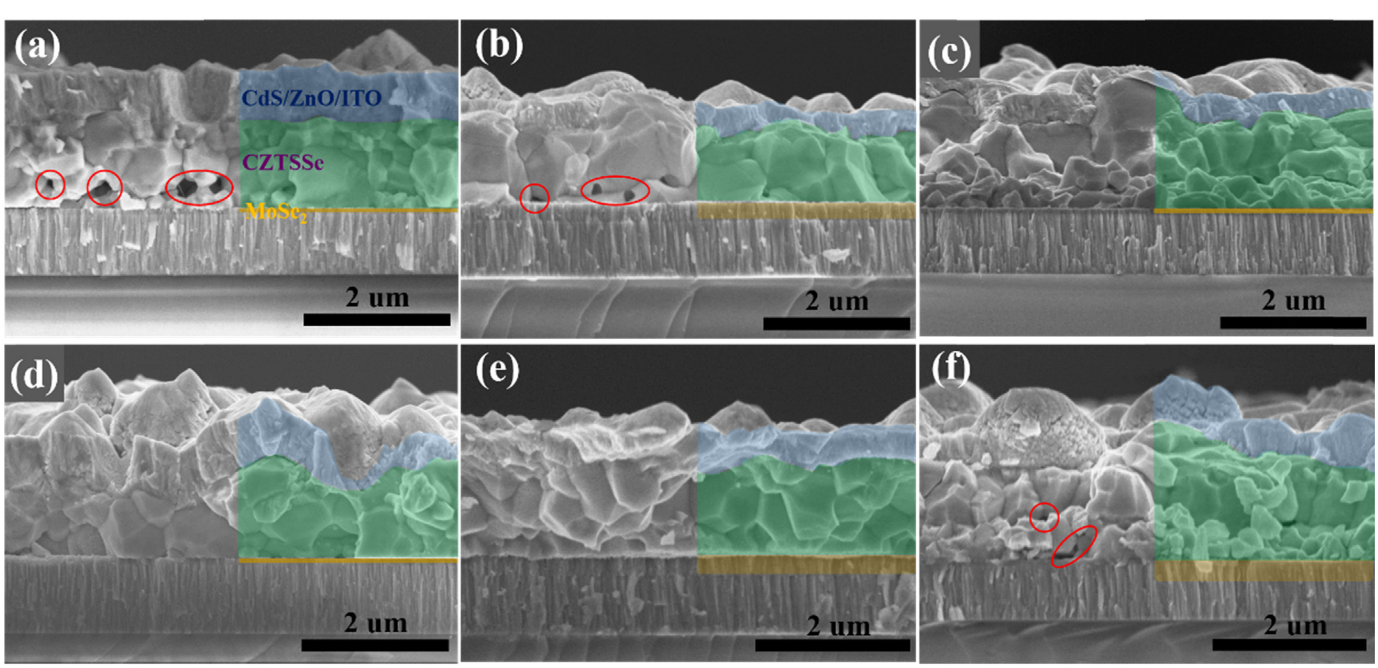

Fig. 7. SEM images of cross-sectional morphology for (a) Cell-I, (b) Cell-II, (c) Cell-III, (d) Cell-IV, (e) Cell-V and (f) Cell-VI.

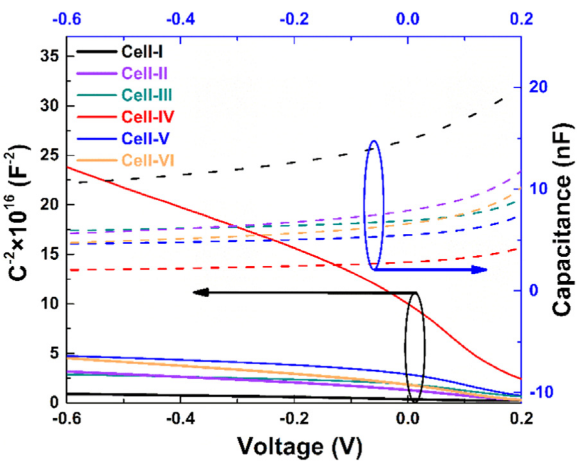

Fig. 8. C-V and C^{-2}-V curves of the CZTSSe solar cells with different cationic ratios.

Table 3
Built-in electric field (V_{bi}), net hole concentrations (N_B) and depletion width (W_d) of the Cell-x (x = I-VI).

Samples	V_{bi} (V)	N_B (cm^{-3})	W_d (nm)
Cell-I	0.60	6.63E+ 16	89.51
Cell-II	0.55	1.76E+ 16	165.69
Cell-III	0.48	1.30E+ 16	180.44
Cell-IV	0.53	2.35E+ 15	448.53
Cell-V	0.81	1.35E+ 16	229.78
Cell-VI	0.50	1.18E+ 16	193.78

Education of China under Grant No. 20120061120011. This work was also supported by Graduate Innovation Fund of Jilin University (No. 2017051) and High Performance Computing Center of Jilin University, China

Appendix A. Supporting information

Supplementary data associated with this article can be found in the online version at doi:10.1016/j.solmat.2019.02.029.

References

[1] W. Wang, M.T. Winkler, O. Gunawan, T. Gokmen, T.K. Todorov, Y. Zhu, D.B. Mitzi, Device Characteristics of CZTSSe Thin-Film Solar Cells with 12.6% Efficiency, Adv. Energy Mater. 4 (2014) 1301465.

[2] S.G. Haass, M. Diethelm, M. Werner, B. Bissig, Y.E. Romanyuk, A.N. Tiwari, 11.2% Efficient solution processed kesterite solar cell with a low voltage deficit, Adv. Energy Mater. 5 (2015) 1500712.

[3] W. Ki, H.W. Hillhouse, Earth-Abundant element photovoltaics directly from soluble precursors with high yield using a non-toxic solvent, Adv. Energy Mater. 1 (2011) 732–735.

[4] H. Xin, J.K. Katahara, I.L. Braly, H.W. Hillhouse, 8% Efficient $Cu_2ZnSn(S,Se)_4$ solar cells from redox equilibrated simple precursors in DMSO, Adv. Energy Mater. 4 (2014) 1301823.

[5] S.H. Wu, K.T. Huang, H.J. Chen, C.F. Shih, $Cu_2ZnSn(S_xSe_{1-x})_4$ thin film solar cell with high sulfur content (x approximately 0.4) and low Voc deficit prepared using a postsulfurization process, Sol. Energy Mater. Sol. Cells 175 (2018) 89–95.

[6] Z. Su, K. Sun, Z. Han, H. Cui, F. Liu, Y. Lai, J. Li, X. Hao, Y. Liu, M.A. Green, Fabrication of Cu_2ZnSnS_4 solar cells with 5.1% efficiency via thermal decomposition and reaction using a non-toxic sol–gel route, J. Mater. Chem. A 2 (2014) 500–509.

[7] Z. Su, J.M.R. Tan, X. Li, X. Zeng, S.K. Batabyal, L.H. Wong, Cation substitution of solution-processed Cu_2ZnSnS_4 thin film solar cell with over 9% efficiency, Adv. Energy Mater. 5 (2015) 1500682.

[8] F. Liu, F. Zeng, N. Song, L. Jiang, Z. Han, Z. Su, C. Yan, X. Wen, X. Hao, Y. Liu, Kesterite $Cu_2ZnSn(S,Se)_4$ solar cells with beyond 8% efficiency by a sol-gel and selenization process, ACS Appl. Mater. Interfaces 7 (2015) 14376–14383.

[9] G. Larramona, S. Levcenko, S. Bourdais, A. Jacob, C. Choné, B. Delatouche, C. Moisan, J. Just, T. Unold, G. Dennler, Fine-tuning the Sn content in CZTSSe thin films to achieve 10.8% solar cell efficiency from spray-deposited water-ethanol-based colloidal inks, Adv. Energy Mater. 5 (2015) 1501404.

[10] M. Jiang, F. Lan, X. Yan, G. Li, $Cu_2ZnSn(S_{1-x}Se_x)_4$ thin film solar cells prepared by water-based solution process, Phys. Status Solidi (RRL) - Rapid Res. Lett. 8 (2014) 223–227.

[11] V. Tunuguntla, W.C. Chen, P.H. Shih, I. Shown, Y.R. Lin, J.S. Hwang, C.H. Lee, L.C. Chen, K.H. Chen, A nontoxic solvent based sol–gel Cu_2ZnSnS_4 thin film for high efficiency and scalable low-cost photovoltaic cells, J. Mater. Chem. A 3 (2015) 15324–15330.

[12] F. Liu, S. Shen, F. Zhou, N. Song, X. Wen, J.A. Stride, K. Sun, C. Yan, X. Hao, Kesterite Cu_2ZnSnS_4 thin film solar cells by a facile DMF-based solution coating process, J. Mater. Chem. C. 3 (2015) 10783–10792.

[13] M.P. Suryawanshi, U.V. Ghorpade, U.P. Suryawanshi, M. He, J. Kim, M.G. Gang, P.S. Patil, A.V. Moholkar, J.H. Yun, J.H. Kim, Aqueous-solution-processed $Cu_2ZnSn(S,Se)_4$ thin-film solar cells via an improved successive ion-layer-adsorption–reaction sequence, ACS Omega 2 (2017) 9211–9220.

[14] T. Schnabel, M. Seboui, E. Ahlswede, Evaluation of different metal salt solutions for the preparation of solar cells with wide-gap $Cu_2ZnGeS_xSe_{4-x}$ absorbers, RSC Adv. 7 (2017) 26–30.

[15] A.D. Collord, H.W. Hillhouse, Germanium alloyed kesterite solar cells with low voltage deficits, Chem. Mater. 28 (2016) 2067–2073.

[16] K. Jimbo, R. Kimura, T. Kamimura, S. Yamada, W.S. Maw, H. Araki, K. Oishi, H. Katagiri, Cu_2ZnSnS_4-type thin film solar cells using abundant materials, Thin Solid Films 515 (2007) 5997–5999.

[17] S. Chen, A. Walsh, X.G. Gong, S.H. Wei, Classification of lattice defects in the kesterite Cu_2ZnSnS_4 and $Cu_2ZnSnSe_4$ earth-abundant solar cell absorbers, Adv. Mater. 25 (2013) 1522–1539.

[18] J. Li, S. Kim, D. Nam, X. Liu, J. Kim, H. Cheong, W. Liu, H. Li, Y. Sun, Y. Zhang, Tailoring the defects and carrier density for beyond 10% efficient CZTSe thin film solar cells, Sol. Energy Mater. Sol. Cells 159 (2017) 447–455.

[19] Y. Ren, M. Richter, J. Keller, A. Redinger, T. Unold, O. Donzel-Gargand, J.J.S. Scragg, C. Platzer Björkman, Investigation of the SnS/Cu_2ZnSnS_4 interfaces in kesterite thin-film solar cells, ACS Energy Lett. 2 (2017) 976–981.

[20] J. Kim, S. Park, S. Ryu, J. Oh, B. Shin, Improving the open-circuit voltage of $Cu_2ZnSnSe_4$ thin film solar cells via interface passivation, Progress. Photovolt.: Res. Appl. 25 (2017) 308–317.

[21] H. Xie, S. Lopez-Marino, T. Olar, Y. Sanchez, M. Neuschitzer, F. Oliva, S. Giraldo, V. Izquierdo-Roca, I. Lauermann, A. Perez-Rodriguez, E. Saucedo, Impact of Na dynamics at the $Cu_2ZnSn(S,Se)_4$/CdS interface during post low temperature treatment of absorbers, ACS Appl. Mater. Interfaces 8 (2016) 5017–5024.

[22] Z.Y. Xiao, B. Yao, Y.F. Li, Z.H. Ding, Z.M. Gao, H.F. Zhao, L.G. Zhang, Z.Z. Zhang, Y.R. Sui, G. Wang, Influencing mechanism of the selenization temperature and time on the power conversion efficiency of $Cu_2ZnSn(S,Se)_4$-based solar cells, ACS Appl. Mater. Interfaces 8 (2016) 17334–17342.

[23] H. Luan, B. Yao, Y. Li, R. Liu, Z. Ding, K. Shi, Y. Li, Z. Zhang, H. Zhao, L. Zhang, Effects of etching on surface structure of $Cu_2ZnSn(S,Se)_4$ absorber and performance of solar cell, Sol. Energy 173 (2018) 696–701.

[24] M. Neuschitzer, Y. Sanchez, S. López-Marino, H. Xie, A. Fairbrother, M. Placidi, S. Haass, V. Izquierdo-Roca, A. Perez-Rodriguez, E. Saucedo, Optimization of CdS buffer layer for high-performance $Cu_2ZnSnSe_4$ solar cells and the effects of light soaking: elimination of crossover and red kink, Prog. Photovolt.: Res. Appl. 23 (2015) 1660–1667.

[25] C.W. Hong, S.W. Shin, M.P. Suryawanshi, M.G. Gang, J. Heo, J.H. Kim, Chemically deposited CdS Buffer/Kesterite Cu_2ZnSnS_4 Solar Cells: relationship between CdS thickness and device performance, ACS Appl. Mater. Interfaces 9 (2017) 36733–36744.

[26] H. Guo, Y. Cui, Q. Tian, S. Gao, G. Wang, D. Pan, Significantly enhancing grain growth in $Cu_2ZnSn(S,Se)_4$ absorber layers by insetting Sb_2S_3, $CuSbS_2$, and $NaSb_5S_8$ thin films, Cryst. Growth Des. 15 (2015) 771–777.

[27] J. Li, D. Wang, X. Li, Y. Zeng, Y. Zhang, Cation substitution in earth-abundant kesterite photovoltaic materials, Adv. Sci. 5 (2018) 1700744.

[28] D. Shin, B. Saparov, D.B. Mitzi, Defect engineering in multinary earth-abundant chalcogenide photovoltaic materials, Adv. Energy Mater. 7 (2017) 1602366.

[29] G. Chen, W. Wang, J. Zhang, S. Chen, Z. Huang, Formation mechanism of secondary phases in Cu_2ZnSnS_4 growth under different copper content, Mater. Lett. 186 (2017) 98–101.

[30] X. Liu, Y. Feng, H. Cui, F. Liu, X. Hao, G. Conibeer, D.B. Mitzi, M. Green, The current status and future prospects of kesterite solar cells: a brief review, Progress. Photovolt.: Res. Appl. 24 (2016) 879–898.

[31] J. Nelson, The Physics of Solar Cells, Imperial College Press CrossRef Google Scholar, UK, 2003.

[32] G. Yang, Y.F. Li, B. Yao, Z.H. Ding, R. Deng, H.F. Zhao, L.G. Zhang, Z.Z. Zhang, Growth of large grain-size $Cu_2ZnSn(S_xSe_{1-x})_4$ thin films by annealing precursors sputtered from a single quaternary target for solar cells application, Superlattices Microstruct. 109 (2017) 480–489.

[33] S.S. Hegedus, W.N. Shafarman, Thin-film solar cells: device measurements and analysis, Prog. Photovolt.: Res. Appl. 12 (2004) 155–176.

[34] M. Saad, A. Kassis, Analysis of illumination-intensity-dependent j–V characteristics of $ZnO/CdS/CuGaSe_2$ single crystal solar cells, Sol. Energy Mater. Sol. Cells 77 (2003) 415–422.

[35] M. Saad, A. Kassis, Effect of interface recombination on solar cell parameters, Sol. Energy Mater. Sol. Cells 79 (2003) 507–517.

[36] A. Kassis, M. Saad, Fill factor losses in $ZnO/CdS/CuGaSe_2$ single-crystal solar cells, Sol. Energy Mater. Sol. Cells 80 (2003) 491–499.

[37] J. Krustok, R. Josepson, M. Danilson, D. Meissner, Temperature dependence of $Cu_2ZnSn(Se_xS_{1-x})_4$ monograin solar cells, Sol. Energy 84 (2010) 379–383.

[38] H.W.S.U. Rau, Electronic properties of $Cu(In,Ga)Se_2$ heterojunction solar ce-recent achievements, current understanding, and future challenges, Appl. Phys. A Mater.

Sci. Process. 69 (1999) 131–147.
[39] T. Gershon, Y.S. Lee, P. Antunez, R. Mankad, S. Singh, D. Bishop, O. Gunawan, M. Hopstaken, R. Haight, Photovoltaic materials and devices based on the alloyed kesterite absorber $(Ag_xCu_{1-x})_2ZnSnSe_4$, Adv. Energy Mater. 6 (2016) 1502468.
[40] O. Gunawan, T.K. Todorov, D.B. Mitzi, Loss mechanisms in hydrazine-processed $Cu_2ZnSn(Se,S)_4$ solar cells, Appl. Phys. Lett. 97 (2010) 233506.
[41] S. Bag, O. Gunawan, T. Gokmen, Y. Zhu, T.K. Todorov, D.B. Mitzi, Low band gap liquid-processed CZTSe solar cell with 10.1% efficiency, Energy Environ. Sci. 5 (2012) 7060.
[42] S. Bag, O. Gunawan, T. Gokmen, Y. Zhu, D.B. Mitzi, Hydrazine-processed Ge-substituted CZTSe solar cells, Chem. Mater. 24 (2012) 4588–4593.
[43] H. Xie, Y. Sanchez, S. Lopez-Marino, M. Espindola-Rodriguez, M. Neuschitzer, D. Sylla, A. Fairbrother, V. Izquierdo-Roca, A. Perez-Rodriguez, E. Saucedo, Impact of Sn(S,Se) secondary phases in $Cu_2ZnSn(S,Se)_4$ solar cells: a chemical route for their selective removal and absorber surface passivation, ACS Appl. Mater. Interfaces 6 (2014) 12744–12751.
[44] J.J. Scragg, T. Kubart, J.T. Wätjen, T. Ericson, M.K. Linnarsson, C. Platzer-Björkman, Effects of back contact instability on Cu_2ZnSnS_4 devices and processes, Chem. Mater. 25 (2013) 3162–3171.
[45] J.J. Scragg, J.T. Watjen, M. Edoff, T. Ericson, T. Kubart, C. Platzer-Bjorkman, A detrimental reaction at the molybdenum back contact in $Cu_2ZnSn(S,Se)_4$ thin-film solar cells, J. Am. Chem. Soc. 134 (2012) 19330–19333.
[46] W.C. Hsu, I. Repins, C. Beall, C. DeHart, G. Teeter, B. To, Y. Yang, R. Noufi, The effect of Zn excess on kesterite solar cells, Sol. Energy Mater. Sol. Cells 113 (2013) 160–164.
[47] D.B. Mitzi, O. Gunawan, T.K. Todorov, D.A. Barkhouse, Prospects and performance limitations for Cu-Zn-Sn-S-Se photovoltaic technology, Philos. Trans. Ser. A, Math. Phys., Eng. Sci. 371 (2013) 20110432.
[48] J. Guo, W. Zhou, Y. Pei, Q. Tian, D. Kou, Z. Zhou, Y. Meng, S. Wu, High efficiency CZTSSe thin film solar cells from pure element solution: a study of additional Sn complement, Sol. Energy Mater. Sol. Cells 155 (2016) 209–215.
[49] J. Fu, Q. Tian, Z. Zhou, D. Kou, Y. Meng, W. Zhou, S. Wu, Improving the performance of solution-processed $Cu_2ZnSn(S,Se)_4$ photovoltaic materials by Cd^{2+} substitution, Chem. Mater. 28 (2016) 5821–5828.
[50] M. Colina, E. Bailo, B. Medina-Rodríguez, R. Kondrotas, Y. Sánchez-González, D. Sylla, M. Placidi, M. Blanes, F. Ramos, A. Cirera, A. Pérez Rodríguez, E. Saucedo, Optimization of ink-jet printed precursors for $Cu_2ZnSn(S,Se)_4$ solar cells, J. Alloy. Compd. 735 (2018) 2462–2470.
[51] R.B.V. Chalapathy, M.G. Gang, C.W. Hong, J.H. Kim, J.S. Jang, J.H. Yun, J.H. Kim, Performance of CZTSSe thin film solar cells fabricated using a sulfo-selenization process: influence of the Cu composition, Sol. Energy 159 (2018) 260–269.
[52] M.G. Gang, S.W. Shin, M.P. Suryawanshi, U.V. Ghorpade, Z. Song, J.S. Jang, J.H. Yun, H. Cheong, Y. Yan, J.H. Kim, Band tail engineering in kesterite $Cu_2ZnSn(S,Se)_4$ thin-film solar cells with 11.8% efficiency, J. Phys. Chem. Lett. 9 (2018) 4555–4561.
[53] C. Li, B. Yao, Y. Li, Z. Ding, H. Zhao, L. Zhang, Z. Zhang, Impact of sequential annealing step on the performance of $Cu_2ZnSn(S,Se)_4$ thin film solar cells, Superlattices Microstruct. 95 (2016) 149–158.
[54] J. Li, H. Wang, M. Luo, J. Tang, C. Chen, W. Liu, F. Liu, Y. Sun, J. Han, Y. Zhang, 10% Efficiency $Cu_2ZnSn(S,Se)_4$ thin film solar cells fabricated by magnetron sputtering with enlarged depletion region width, Sol. Energy Mater. Sol. Cells 149 (2016) 242–249.